CRAMÉR-RAO BOUND ANALYSIS ON MULTIPLE SCATTERING IN MULTISTATIC POINT SCATTERER ESTIMATION

Gang Shi and Arye Nehorai

Department of Electrical and Systems Engineering
Washington University in St. Louis
St. Louis, MO 63130

ABSTRACT

The resolution improvements of time reversal methods through exploiting nonhomogeneous media have attracted much interest recently with broad applications, including the destruction of kidney stones, underwater acoustics, radar, detection of defects in metals, communications, and mine detection. In this paper, we analyze the effect of inhomogeneity generated by multiple scattering among point scatterers under a multistatic sensing setup. We derive the Cramér-Rao bounds (CRBs) on parameters of the scatterers and compare the CRBs for multiple scattering using the Foldy-Lax model with the reference case without multiple scattering using the Born approximation. We find that multiple scattering could significantly improve the estimation performance of the system. For the case where multiple scattering is not possible, e.g., where only a single target scatterer exists in the illuminated scenario, we propose the use of *artificial scatterers*, which could effectively improve the estimation performance of the target despite a decrease in the degrees of freedom of the estimation problem due to the introduced unknown parameters of the artificial scatterers. Numerical examples demonstrate the advantage of the artificial scatterer.

1. INTRODUCTION

The time reversal approach and its super resolution [1] have attracted increasing interest recently with broad applications, including the destruction of kidney stones, underwater acoustics, radar, detection of defects in metals, communications, and mine detection. The idea behind so-called *physical time reversal* is to record a signal emitted by sources or reflected by targets using an array of transducers and then transmit the time-reversed and complex conjugated version of the measurements back into the medium. In a reciprocal medium, the back-propagated wave will then retrace the original trajectory and focus around the original source locations. Experimental and theoretical evidence shows [2], [3] that the refocusing in a non-homogeneous or random medium is much tighter than in homogeneous, which is referred to as the *super-resolution* of the time reversal. This super-resolution is intuitively interpreted as taking advantage of the inhomogeneity to distribute the wave over a larger part of the medium and therefore carry more information about the source, and it is quantitatively measured as the improved *effective aperture* [4], which corresponds to the equivalent aperture that produces the same refocusing resolution in a reference homogeneous medium.

This work was supported by the DARPA/AFOSR grant FA9550-04-1-0187 and AFOSR grant FA9550-05-1-0018.

Encouraged by results in the situation of inhomogeneity, we investigate possible advantages of multiple scattering in point scattering estimation, in which the inhomogeneity is induced by interactions of the scatterers. Multiple scattering exists in many physical systems involving wave propagation, including electrons, ultrasound, electromagnetic, and seismic waves, and can be analyzed using very much the same concepts [5]. Though modeling and understanding of multiple scattering has been of interest in various domains ranging from solid-state physics to optics to seismology [6], it is still widely ignored in the signal processing literature, to the best of the authors' knowledge. Recently, MUSIC and maximum likelihood (ML) algorithms for estimating the locations of point scatterers with multiple scattering were proposed in [7]-[10]. Cramér-Rao Bounds (CRBs) are computed in [11] to evaluate the performance of reflectivity estimation in an unknown environment using physical time reversal. In this paper, we continue our work in [9], [10] by evaluating the effect of multiple scattering on the performance of point scatter estimation. We will evaluate multiple scattering under an active multistatic sensing setup without physical time reversal, and measure the performance in terms of the well-known performance benchmark CRB.

This paper is organized as follows: In Section 2, we present two physical models used in later comparisons: one takes into account the multiple scattering among the scatterers using the Foldy-Lax model [12], and the other ignores it by using the Born approximation [12], [13]. In Section 3, we compute the CRBs based on these two physical models, and then present numerical evaluations of the CRBs under randomized setups in Section 4. In Section 5, we propose the use of artificial scatterers to improve the system performance and present conclusions in Section 6. Due to the space limitation, interested readers are referred to the journal version of this paper [14] for more detailed discussions and proofs of the results.

2. PHYSICAL AND MEASUREMENT MODELS

We consider a transmit antenna array of N_{t} isotropic point antennas centered at known positions $\boldsymbol{\alpha}_1, \boldsymbol{\alpha}_2, \ldots, \boldsymbol{\alpha}_{N_{\mathrm{t}}}$, and a receive array of N_{r} elements at $\boldsymbol{\beta}_1, \boldsymbol{\beta}_2, \ldots, \boldsymbol{\beta}_{N_{\mathrm{r}}}$. The so-called $N_{\mathrm{r}} \times N_{\mathrm{t}}$ *multistatic response matrix* [15], [16] $K = [K_{j,k}(\omega)]$, represented in the frequency domain is a function of the frequency ω whose element $K_{j,k}(\omega)$ coincides with the received signal at the j-th receive antenna due to an impulse excitation applied by the k-th transmit antenna, where $j = 1, 2, \ldots, N_{\mathrm{r}}$ and $k = 1, 2, \ldots, N_{\mathrm{t}}$. We assume the scenario under probe is stationary during the period of sensing and there is no direct link from any transmit antenna to the receive antennas, i.e., the measured fields at the receive array are due solely to the scattering of the illuminated scenario. Since the information about the scenario is fully embedded in the multistatic matrix, the inference on the probed scenario will be based on the measured multistatic matrix directly. We consider the scenario that consists of M discrete point scatterers in a background medium with known Green function $G(\boldsymbol{r}, \boldsymbol{r}', \omega)$. The unknown locations and scattering potentials of the scatterers are denoted by $\boldsymbol{x}_1, \boldsymbol{x}_2, \ldots, \boldsymbol{x}_M$ and $\tau_1(\omega), \tau_2(\omega), \ldots, \tau_M(\omega)$, respectively. The time harmonic Green function $G(\boldsymbol{r}, \boldsymbol{r}', \omega)$ of the background, which represents the "propagator" at ω from location $\boldsymbol{r}'$ to $\boldsymbol{r}$, satisfies the reduced wave equation [15]. In the rest of this paper, we will drop the dependence on ω in all notations for the sake of simplicity.

Adopting the Foldy-Lax multiple scattering equations [12], we formulate the multistatic matrix in a closed matrix form [9], [10]

$$K_{\mathrm{FL}}(\boldsymbol{x}, \boldsymbol{\tau}) \;=\; A_{\mathrm{r}}(\boldsymbol{x})[T^{-1}(\boldsymbol{\tau}) - S(\boldsymbol{x})]^{-1} A_{\mathrm{t}}^T(\boldsymbol{x}), \qquad (1)$$

where "^{T}" stands for a matrix transpose, $\boldsymbol{x} = [\boldsymbol{x}_1^T, \boldsymbol{x}_2^T, \ldots, \boldsymbol{x}_M^T]^T \in \mathbb{R}^{3M}$ representing the unknown location parameters, $\boldsymbol{\tau} = [\tau_1, \tau_2, \ldots, \tau_M]^T \in \mathbb{C}^M$ unknown scattering parameters, and $T(\boldsymbol{\tau}) = \mathrm{diag}\{\boldsymbol{\tau}\}$. The matrix $S(\boldsymbol{x})$ is defined as $S(\boldsymbol{x}) =$

$$\begin{bmatrix} 0 & G(\boldsymbol{x}_1, \boldsymbol{x}_2) & & \cdots & G(\boldsymbol{x}_1, \boldsymbol{x}_M) \\ G(\boldsymbol{x}_2, \boldsymbol{x}_1) & 0 & & \cdots & G(\boldsymbol{x}_2, \boldsymbol{x}_M) \\ \vdots & & \ddots & & \vdots \\ G(\boldsymbol{x}_{M-1}, \boldsymbol{x}_1) & \cdots & & 0 & G(\boldsymbol{x}_{M-1}, \boldsymbol{x}_M) \\ G(\boldsymbol{x}_M, \boldsymbol{x}_1) & \cdots & & G(\boldsymbol{x}_M, \boldsymbol{x}_{M-1}) & 0 \end{bmatrix},$$

and $A_{\mathrm{r}}(\boldsymbol{x}) = [\boldsymbol{g}_{\mathrm{r}}(\boldsymbol{x}_1), \boldsymbol{g}_{\mathrm{r}}(\boldsymbol{x}_2) \cdots \boldsymbol{g}_{\mathrm{r}}(\boldsymbol{x}_M)]$, $A_{\mathrm{t}}(\boldsymbol{x}) = [\boldsymbol{g}_{\mathrm{t}}(\boldsymbol{x}_1), \boldsymbol{g}_{\mathrm{t}}(\boldsymbol{x}_2) \cdots \boldsymbol{g}_{\mathrm{t}}(\boldsymbol{x}_M)]$; the receive Green function vector $\boldsymbol{g}_{\mathrm{r}}(\boldsymbol{x}') \in \mathbb{C}^{N_{\mathrm{r}}}$ as a function of arbitrary location $\boldsymbol{x}' \in \mathbb{R}^3$ is $\boldsymbol{g}_{\mathrm{r}}(\boldsymbol{x}') = [G(\boldsymbol{\beta}_1, \boldsymbol{x}'), G(\boldsymbol{\beta}_2, \boldsymbol{x}'), \ldots, G(\boldsymbol{\beta}_{N_{\mathrm{r}}}, \boldsymbol{x}')]^T$ and the transmit Green function vector $\boldsymbol{g}_{\mathrm{t}}(\boldsymbol{x}') \in \mathbb{C}^{N_{\mathrm{t}}}$ is $\boldsymbol{g}_{\mathrm{t}}(\boldsymbol{x}') = [G(\boldsymbol{x}', \boldsymbol{\alpha}_1), G(\boldsymbol{x}', \boldsymbol{\alpha}_2), \ldots, G(\boldsymbol{x}', \boldsymbol{\alpha}_{N_{\mathrm{t}}})]^T$. Note that the closed-form matrix representation (1) is a function of the background Green function only.

Using the identity $(I - A)^{-1} = I + A + A^2 + \cdots$, the multistatic matrix (1) can be expanded into the power series as

$$\begin{aligned} K_{\mathrm{FL}}(\boldsymbol{x}, \boldsymbol{\tau}) &= A_{\mathrm{r}}(\boldsymbol{x}) T(\boldsymbol{\tau}) A_{\mathrm{t}}^T(\boldsymbol{x}) + A_{\mathrm{r}}(\boldsymbol{x}) T(\boldsymbol{\tau}) S(\boldsymbol{x}) T(\boldsymbol{\tau}) A_{\mathrm{t}}^T(\boldsymbol{x}) \\ &\quad + A_{\mathrm{r}}(\boldsymbol{x}) T(\boldsymbol{\tau}) S(\boldsymbol{x}) T(\boldsymbol{\tau}) S(\boldsymbol{x}) T(\boldsymbol{\tau}) A_{\mathrm{t}}^T(\boldsymbol{x}) + \cdots. \qquad (2) \end{aligned}$$

This series form is actually a generalization of the Neumann series or Born series [12], [13] under the multistatic context, and its convergence is guaranteed when the spectral radius of $T(\boldsymbol{\tau})S(\boldsymbol{x})$ is less than one. The leading term of (2), known as the Born approximation, represents the first-order scattering, i.e., the scattering without taking into account the multiple scattering. The second term represents the second-order scattering contribution, namely the portion of the scattering that is reflected by the scatterers exactly twice. The rest of the series are higher order scattering terms. We will employ the Born-approximated model

$$K_{\mathrm{B}}(\boldsymbol{x}, \boldsymbol{\tau}) = A_{\mathrm{r}}(\boldsymbol{x}) T(\boldsymbol{\tau}) A_{\mathrm{t}}^T(\boldsymbol{x}) \qquad (3)$$

as the reference model for studying the effect of multiple scattering on the estimation performance. It is easy to see that the model (3) is a special case of (1) when the $S(\boldsymbol{x})$ matrix is set to be zero matrix.

Before computing the CRBs, we further assume that Y, the measured the multistatic matrix, deviates from the model $K(\boldsymbol{x}, \boldsymbol{\tau})$ by additive independent, identically distributed (i.i.d.) complex circularly symmetric Gaussian noise, i.e.,

$$Y = K(\boldsymbol{x}, \boldsymbol{\tau}) + W, \qquad (4)$$

where W is $N_{\mathrm{r}} \times N_{\mathrm{t}}$ noise matrix whose elements $\mathrm{vec}(W) \sim \mathcal{CN}(\boldsymbol{0}, \sigma^2 I_{N_{\mathrm{r}}N_{\mathrm{t}}})$ and $\mathrm{vec}(\cdot)$ stacks the first to the last columns of the matrix one under another to form a long vector. It worth mentioning that though it is technically feasible to derive the CRBs under a more general correlated noise model, the simple noise assumption is for gaining insight into the differences between the two scattering processes with and without multiple scattering, respectively.

3. CRAMÉR-RAO BOUND RESULTS

We start deriving the CRBs [17] from the expression for the Fisher information matrix (FIM) in [18]. Reparameterizing the unknown scattering parameters $\boldsymbol{\tau}$ into real parameters $\tilde{\boldsymbol{\tau}} = [\mathrm{Re}\{\tau_1\}, \mathrm{Im}\{\tau_1\}, \ldots, \mathrm{Re}\{\tau_M\}, \mathrm{Im}\{\tau_M\}]^T \in \mathbb{R}^{2M}$, where $\mathrm{Re}\{\cdot\}$ and $\mathrm{Im}\{\cdot\}$ denote the real and imaginary parts of a complex number, respectively. Define $\boldsymbol{\theta} = [\tilde{\boldsymbol{\tau}}^T, \boldsymbol{x}^T]^T$, and the FIM for $\boldsymbol{\theta}$ is found as

$$\begin{aligned} \mathcal{I}(\boldsymbol{\theta}) &= \frac{2}{\sigma^2} \mathrm{Re}\Big\{ \Big[\frac{\partial \mathrm{vec}\big(K(\boldsymbol{x}, \boldsymbol{\tau})\big)}{\partial \boldsymbol{\theta}^T} \Big]^H \Big[\frac{\partial \mathrm{vec}\big(K(\boldsymbol{x}, \boldsymbol{\tau})\big)}{\partial \boldsymbol{\theta}^T} \Big] \Big\} \\ &= \frac{2}{\sigma^2} \mathrm{Re}\big\{ D^H(\boldsymbol{\theta}) D(\boldsymbol{\theta}) \big\}, \qquad (5) \end{aligned}$$

where "^{H}" represents the conjugate transpose. The Jacobian matrix $D(\boldsymbol{\theta}) = \partial \mathrm{vec}\big(K(\boldsymbol{x}, \boldsymbol{\tau})\big)/\partial \boldsymbol{\theta}^T$ could be partitioned as $D(\boldsymbol{\theta}) = [D_{\tilde{\boldsymbol{\tau}}},\ D_{\boldsymbol{x}}]$, where $D_{\tilde{\boldsymbol{\tau}}} = \partial \mathrm{vec}\big(K(\boldsymbol{x}, \boldsymbol{\tau})\big)/\partial \tilde{\boldsymbol{\tau}}^T$ and $D_{\boldsymbol{x}} = \partial \mathrm{vec}\big(K(\boldsymbol{x}, \boldsymbol{\tau})\big)/\partial \boldsymbol{x}^T$. Following the same partition, the FIM is partitioned accordingly as

$$\mathcal{I}(\boldsymbol{\theta}) = \begin{bmatrix} \mathcal{I}_{\tilde{\boldsymbol{\tau}}\tilde{\boldsymbol{\tau}}} & \mathcal{I}_{\boldsymbol{x}\tilde{\boldsymbol{\tau}}}^T \\ \mathcal{I}_{\boldsymbol{x}\tilde{\boldsymbol{\tau}}} & \mathcal{I}_{\boldsymbol{x}\boldsymbol{x}} \end{bmatrix}. \qquad (6)$$

The CRB matrix for location parameters $\boldsymbol{x}$ is

$$\mathrm{CRB}(\boldsymbol{x}; \tilde{\boldsymbol{\tau}}) = (\mathcal{I}_{\boldsymbol{x}\boldsymbol{x}} - \mathcal{I}_{\boldsymbol{x}\tilde{\boldsymbol{\tau}}} \mathcal{I}_{\tilde{\boldsymbol{\tau}}\tilde{\boldsymbol{\tau}}}^{-1} \mathcal{I}_{\boldsymbol{x}\tilde{\boldsymbol{\tau}}}^T)^{-1}, \qquad (7)$$

and the CRB matrix for scattering parameter $\tilde{\boldsymbol{\tau}}$ is

$$\mathrm{CRB}(\tilde{\boldsymbol{\tau}}; \boldsymbol{x}) = (\mathcal{I}_{\tilde{\boldsymbol{\tau}}\tilde{\boldsymbol{\tau}}} - \mathcal{I}_{\boldsymbol{x}\tilde{\boldsymbol{\tau}}}^T \mathcal{I}_{\boldsymbol{x}\boldsymbol{x}}^{-1} \mathcal{I}_{\boldsymbol{x}\tilde{\boldsymbol{\tau}}})^{-1}. \qquad (8)$$

For the case *with multiple scattering*, the Jacobian matrices $D_{\mathrm{FL}\tilde{\boldsymbol{\tau}}}$ and $D_{\mathrm{FL}\boldsymbol{x}}$ are found as

$$\begin{aligned} D_{\mathrm{FL}\tilde{\boldsymbol{\tau}}} &= \big(A_{\mathrm{t}}(\boldsymbol{x}) [I_M - T(\boldsymbol{\tau}) S(\boldsymbol{x})]^{-1} \\ &\qquad \odot A_{\mathrm{r}}(\boldsymbol{x}) [I_M - T(\boldsymbol{\tau}) S(\boldsymbol{x})]^{-1} \big) \otimes (1, i), \qquad (9) \\ D_{\mathrm{FL}\boldsymbol{x}} &= \big(A_{\mathrm{t}}(\boldsymbol{x}) [T^{-1}(\boldsymbol{\tau}) - S(\boldsymbol{x})]^{-1} \otimes \mathbf{1}_n^T \big) \odot B_{\mathrm{r}}(\boldsymbol{x}) \\ &\quad - \big(A_{\mathrm{t}}(\boldsymbol{x}) [T^{-1}(\boldsymbol{\tau}) - S(\boldsymbol{x})]^{-1} \otimes A_{\mathrm{r}}(\boldsymbol{x}) [T^{-1}(\boldsymbol{\tau}) - S(\boldsymbol{x})]^{-1} \big) C(\boldsymbol{x}) \\ &\quad + B_{\mathrm{t}}(\boldsymbol{x}) \odot \big(A_{\mathrm{r}}(\boldsymbol{x}) [T^{-1}(\boldsymbol{\tau}) - S(\boldsymbol{x})]^{-1} \otimes \mathbf{1}_n^T \big), \qquad (10) \end{aligned}$$

where

- "$\odot$" stands for the Khatri-Rao product [19],
- "$\otimes$" represents the Kronecker product [19],
- "i" is the imaginary unit,
- $B_{\mathrm{t}}(\boldsymbol{x}) = [\boldsymbol{b}_{\mathrm{t}}(\boldsymbol{x}_1), \boldsymbol{b}_{\mathrm{t}}(\boldsymbol{x}_2) \cdots \boldsymbol{b}_{\mathrm{t}}(\boldsymbol{x}_M)]$,
- $\boldsymbol{b}_{\mathrm{t}}(\boldsymbol{x}_m) = \partial \boldsymbol{g}_{\mathrm{t}}(\boldsymbol{x}_m)/\partial \boldsymbol{x}_m^T$, $m = 1, 2, \ldots, M$,

- $B_{\mathrm{r}}(\boldsymbol{x}) = [\boldsymbol{b}_{\mathrm{r}}(\boldsymbol{x}_1), \boldsymbol{b}_{\mathrm{r}}(\boldsymbol{x}_2) \cdots \boldsymbol{b}_{\mathrm{r}}(\boldsymbol{x}_M)]$,
- $\boldsymbol{b}_{\mathrm{r}}(\boldsymbol{x}_m) = \partial \boldsymbol{g}_{\mathrm{r}}(\boldsymbol{x}_m)/\partial \boldsymbol{x}_m^T$, $m = 1, 2, \ldots, M$,
- $\mathbf{1}_n$: n-dimension column vector with each element as 1,
- n is the dimension of one location parameter $\boldsymbol{x}_m$,
- $C(\boldsymbol{x}) = [\boldsymbol{c}^T(\boldsymbol{x}_1), \boldsymbol{c}^T(\boldsymbol{x}_2) \cdots \boldsymbol{c}^T(\boldsymbol{x}_M)]^T$,
- $\boldsymbol{c}(\boldsymbol{x}_m) = \partial \boldsymbol{g}(\boldsymbol{x}_m)/\partial \boldsymbol{x}^T$, $m = 1, 2, \ldots, M$,
- $\boldsymbol{g}(\boldsymbol{x}_m) = [G(\boldsymbol{x}_1, \boldsymbol{x}_m), G(\boldsymbol{x}_2, \boldsymbol{x}_m), \ldots, G(\boldsymbol{x}_M, \boldsymbol{x}_m)]^T$, in which $G(\boldsymbol{x}_m, \boldsymbol{x}_m) \triangleq 0$, $m = 1, 2, \ldots, M$.

For the reference case *with no multiple scattering*, recalling that multistatic model (3) is the special case of (1), we can find the Jacobian matrices $D_{\mathrm{B}\tilde{\boldsymbol{\tau}}}$ and $D_{\mathrm{B}\boldsymbol{x}}$ by substituting $S(\boldsymbol{x})$ as a zero matrix into (9) and (10), which are

$$D_{\mathrm{B}\tilde{\boldsymbol{\tau}}} = A_{\mathrm{t}}(\boldsymbol{x}) \odot A_{\mathrm{r}}(\boldsymbol{x}) \otimes (1, i), \tag{11}$$

$$\begin{aligned} D_{\mathrm{B}\boldsymbol{x}} &= [A_{\mathrm{t}}(\boldsymbol{x}) T(\boldsymbol{\tau}) \otimes \mathbf{1}_n^T] \odot B_{\mathrm{r}}(\boldsymbol{x}) \\ &\quad + B_{\mathrm{t}}(\boldsymbol{x}) \odot [A_{\mathrm{r}}(\boldsymbol{x}) T(\boldsymbol{\tau}) \otimes \mathbf{1}_n^T]. \end{aligned} \tag{12}$$

4. NUMERICAL COMPARISONS

We employ a homogeneous two-dimensional setup, i.e., $n = 2$, the inhomogeneity is then due solely to the multiple scattering among the scatterers. Dropping the unessential constant, we obtain background Green function $G(\boldsymbol{r}, \boldsymbol{r}') = e^{i2\pi|\boldsymbol{r}-\boldsymbol{r}'|/\lambda} / \sqrt{2\pi|\boldsymbol{r}-\boldsymbol{r}'|/\lambda}$ under usual approximation [20]. Assume collocated transmit and receive arrays are uniform linear arrays (ULAs) located between (-20,0) and (20,0) with spacing of 5, i.e., $N_{\mathrm{t}} = N_{\mathrm{r}} = 9$. All the coordinates are in the unit of wavelength, i.e., we assume the narrowband signal with $\lambda = 1$. Detailed discussions on the spatial ambiguity of this sparse setup could be found in [10], whereas we use the 5λ antenna spacing here and [14] is solely for computational simplicity, it is easy to verify that all the results hold for transmit and receive arrays with $\lambda/2$ spacing. Due to the space limitation, more numerical examples are presented in the journal version of this paper [14].

We computed the CRBs on the location and scattering parameters under randomized scatterer setup assuming that three scatterers ($M = 3$) are located randomly and uniformly over a rectangular area centered at $(0, 30)$ with dimension 50×40. Moduli of the scattering potentials were assumed to be independently and uniformly distributed over $[0.5, 1]$, and the phases uniformly distributed over $[0, 2\pi]$. We ran 251 Monte Carlo runs and plot each run as one point in Figure 1 with $\mathrm{tr}\,\mathrm{CRB}_{\mathrm{B}}(\boldsymbol{x}; \tilde{\boldsymbol{\tau}}) / \mathrm{tr}\,\mathrm{CRB}_{\mathrm{FL}}(\boldsymbol{x}; \tilde{\boldsymbol{\tau}})$ as its x coordinate and $\mathrm{tr}\,\mathrm{CRB}_{\mathrm{B}}(\tilde{\boldsymbol{\tau}}; \boldsymbol{x}) / \mathrm{tr}\,\mathrm{CRB}_{\mathrm{FL}}(\tilde{\boldsymbol{\tau}}; \boldsymbol{x})$ as the y coordinate, where "tr" represents the trace of a matrix. If we set point $(1, 1)$ as the coordinate origin, we can see in Figure 1 that all the 251 Monte-Carlo runs are in the first quadrant, which means that multiple scattering improves the CRBs in the randomized setups. The median of $\mathrm{tr}\,\mathrm{CRB}_{\mathrm{B}}(\boldsymbol{x}; \tilde{\boldsymbol{\tau}}) / \mathrm{tr}\,\mathrm{CRB}_{\mathrm{FL}}(\boldsymbol{x}; \tilde{\boldsymbol{\tau}})$ is 7.1254, and 8.6120 for $\mathrm{tr}\,\mathrm{CRB}_{\mathrm{B}}(\tilde{\boldsymbol{\tau}}; \boldsymbol{x}) / \mathrm{tr}\,\mathrm{CRB}_{\mathrm{FL}}(\tilde{\boldsymbol{\tau}}; \boldsymbol{x})$. In addition, a strong positive correlation between the two CRB ratios of $\boldsymbol{x}$ and $\boldsymbol{\tau}$ may be seen in Figure 1, which indicates that the estimation accuracy on the location parameters greatly affects that on the scattering parameters.

It worth mentioning that the favorable effect of multiple scattering on the estimation performance depends on the system setup. For example, if we increase the scattering potentials until the interactions among the scatterers are large enough, the multiple scattering actually turns out to deteriorate the estimation performance.

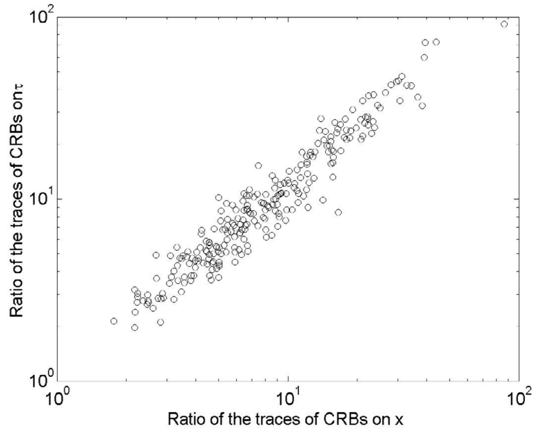

Fig. 1. $\mathrm{tr}\,\mathrm{CRB}_{\mathrm{B}}(\tilde{\boldsymbol{\tau}}; \boldsymbol{x}) / \mathrm{tr}\,\mathrm{CRB}_{\mathrm{FL}}(\tilde{\boldsymbol{\tau}}; \boldsymbol{x})$ versus $\mathrm{tr}\,\mathrm{CRB}_{\mathrm{B}}(\boldsymbol{x}; \tilde{\boldsymbol{\tau}}) / \mathrm{tr}\,\mathrm{CRB}_{\mathrm{FL}}(\boldsymbol{x}; \tilde{\boldsymbol{\tau}})$ in the 251 Monte-Carlo runs.

Identifying conditions under which multiple scattering is beneficial in terms of improving the CRBs is an interesting challenge, which we will consider in our future work.

5. ARTIFICIAL SCATTERERS

One straightforward way of exploiting the advantage of the multiple scattering is simply to introduce it into the modeling. We further propose the use of *artificial scatterers* [21] to create multiple scattering. The artificial scatterers can either be *active* or *passive*: active artificial scatterers could be relays that simply amplify and retransmit the incident wave; passive artificial scatterers could be scatterers that reflect efficiently. The artificial scatterers could be deployed in the scenario of interest in a planned manner or happen to be nearby by opportunity. We use the following numerical examples to demonstrate the efficacy of the artificial scatterers assuming the location and scattering potentials of the deployed artificial scatterers are *unknown*.

The array setup is the same as in Section 4 in which we consider one target scatterer and two artificial scatterers. We compute the traces of the CRBs on the target location $\boldsymbol{x}_1$ and scattering parameters τ_1 for the case without artificial scatterers, denoted by $\mathrm{tr}\,\mathrm{CRB}_1(\boldsymbol{x}_1; \tilde{\tau}_1)$ and $\mathrm{tr}\,\mathrm{CRB}_1(\tilde{\tau}_1; \boldsymbol{x}_1)$, respectively, where $\tilde{\tau}_1 = [\mathrm{Re}\{\tau_1\}, \mathrm{Im}\{\tau_1\}]^T$, then compute the traces of the CRBs of the target scatterer after deploying two artificial scatterers, denoted by $\mathrm{tr}\,\mathrm{CRB}_{1+2}(\boldsymbol{x}_1; \tilde{\tau}_1)$ and $\mathrm{tr}\,\mathrm{CRB}_{1+2}(\tilde{\tau}_1; \boldsymbol{x}_1)$. We plot 251 Monte-Carlo runs with $\mathrm{tr}\,\mathrm{CRB}_1(\boldsymbol{x}_1; \tilde{\tau}_1) / \mathrm{tr}\,\mathrm{CRB}_{1+2}(\boldsymbol{x}_1; \tilde{\tau}_1)$ as x coordinates and $\mathrm{tr}\,\mathrm{CRB}_1(\tilde{\tau}_1; \boldsymbol{x}_1) / \mathrm{tr}\,\mathrm{CRB}_{1+2}(\tilde{\tau}_1; \boldsymbol{x}_1)$ as y coordinates.

In Figure 2 the computation is performed based on Born approximation model (3), as expected all the runs appear in the third quadrant which means that the added artificial scatterers decrease the estimation performance of the single scatterer in the case without multiple scattering. This is the direct consequence of the increased unknown parameters, thus reducing the degrees of freedom of the estimation problem. In Figure 3, the CRBs are computed using the Foldy-Lax model (1). It is interesting to see that most of the Monte-Carlo runs lie in the first quadrant in this case, meaning that the two randomly deployed artificial scatterers improved the estimation performance on the target scatterer via the created multiple scattering. The median of $\operatorname{tr}\mathrm{CRB}_1(\boldsymbol{x}_1;\tilde{\tau}_1)$ / $\operatorname{tr}\mathrm{CRB}_{1+2}(\boldsymbol{x}_1;\tilde{\tau}_1)$ is 6.6418, and 7.9206 for $\operatorname{tr}\mathrm{CRB}_1(\tilde{\tau}_1;\boldsymbol{x}_1)$ / $\operatorname{tr}\mathrm{CRB}_{1+2}(\tilde{\tau}_1;\boldsymbol{x}_1)$. The multiple scattering surprisingly not only offsets the degradation of the CRBs on the target scatterers due the lowered degrees of freedom, but also improves the estimation performance further in most of the randomized scatterer setups.

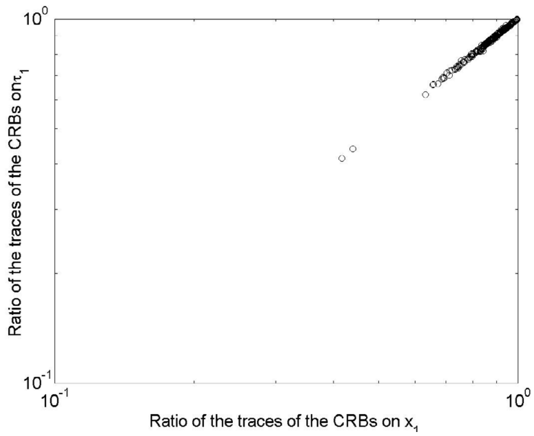

Fig. 2. $\operatorname{tr}\mathrm{CRB}_1(\tilde{\tau}_1;\boldsymbol{x}_1)/\operatorname{tr}\mathrm{CRB}_{1+2}(\tilde{\tau}_1;\boldsymbol{x}_1)$ versus $\operatorname{tr}\mathrm{CRB}_1(\boldsymbol{x}_1;\tilde{\tau}_1)/\operatorname{tr}\mathrm{CRB}_{1+2}(\boldsymbol{x}_1;\tilde{\tau}_1)$ in the absence of multiple scattering.

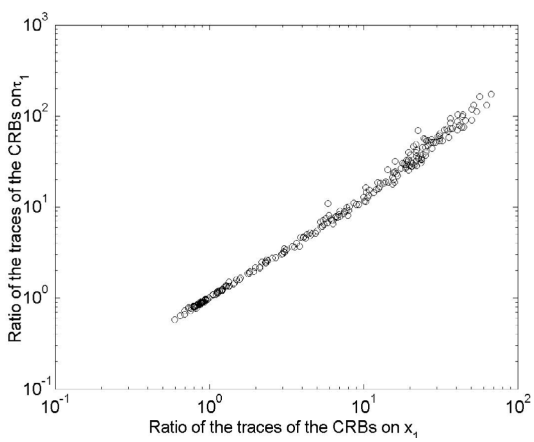

Fig. 3. $\operatorname{tr}\mathrm{CRB}_1(\tilde{\tau}_1;\boldsymbol{x}_1)/\operatorname{tr}\mathrm{CRB}_{1+2}(\tilde{\tau}_1;\boldsymbol{x}_1)$ versus $\operatorname{tr}\mathrm{CRB}_1(\boldsymbol{x}_1;\tilde{\tau}_1)/\operatorname{tr}\mathrm{CRB}_{1+2}(\boldsymbol{x}_1;\tilde{\tau}_1)$ in the presence of multiple scattering.

6. CONCLUSIONS

We derived the Cramér-Rao bounds on the location and scattering parameters of point scatterers under a multistatic sensing setup for the cases in which multiple scattering either exist or not. We demonstrated that the inhomogeneity induced by the multiple scattering could greatly improve the estimation performance in terms of the CRBs. We then proposed the use of artificial scatterers in the absence of natural multiple scattering. Analytically comparing the CRBs in terms of their trace, determinant, or any matrix norm is challenging due to the nonlinear dependence of the CRB matrices on the system parameters. We will investigate this point in our future work.

7. REFERENCES

[1] M. Fink, “Time-reversed acoustics,” *Scientific American*, Nov. 1999.

[2] M. Fink, D. Cassereau, A. Derode, C. Prada, P. Roux, M. Tanter, J. L. Thomas, and F. Wu, “Time-reversed acoustics,” *Rep. Progr. Phys.*, vol. 63, pp. 1933-1995, 2000.

[3] M. Fink and C. Prada. “Acoustic time-reversal mirrors, topical review,” *Inverse Problems*, 17:R1-R38, 2001.

[4] L. Borcea, G. Papanicolaou, and C. Tsogka, “Theory and applications of time reversal and interferometric imaging,” *Inverse Problems*, vol. 19, pp. 5139-5164, 2003.

[5] A. Derode, A. Tourin, and M. Fink, “Random multiple scattering of ultrasound. I. Coherent and ballistic waves,” *Physical Review E*, vol. 64, 036605, 2001.

[6] A. Derode, A. Tourin, and M. Fink, “Random multiple scattering of ultrasound. II. Is time reversal a self-averaging process?” *Physical Review E*, vol. 64, 036606, 2001.

[7] F. K. Gruber, E. A. Marengo, and A. J. Devaney, “Time-reversal imaging with multiple signal classification considering multiple scattering between the targets,” *J. Acoust. Soc. Am.* 115, pp. 3042-3047, June 2004.

[8] A. J. Devaney, E. A. Marengo, and F. K. Gruber, “Time-reversal based imaging and inverse scattering of multiple scattering point targets,” *J. Acoust. Soc. Am.* , to appear.

[9] G. Shi, A. Nehorai, “Maximum likelihood estimation of point scatterers for computational time-reversal imaging,” *Proc. 13th Annu. Workshop on Adaptive Sensor Array Processing*, Lincoln Laboratory, MIT, Lexington, MA, June 2005.

[10] G. Shi, A. Nehorai, “Maximum likelihood estimation of point scatterers for computational time-reversal imaging,” *Communications in Information and Systems,* vol. 5, no. 2, pp. 227-256, 2005.

[11] R. Rangarajan and A. O. Hero III, “Analysis of a multistatic adaptive target illumination and detection approach (MATILDA) to time reversal imaging,” *IMA “Hot Topics” Workshop: Adaptive Sensing and Multimode Data Inversion*, June 27-30, 2004.

[12] J. H. Taylor, *Scattering Theory*, New York, Wiley, 1972.

[13] R. G. Newton, *Scattering Theory of Waves and Particles,* New York, McGraw-Hill, 1966.

[14] G. Shi and A. Nehorai, “Cramér-Rao Bound Analysis on Multiple Scattering in Multistatic Point Scatterer Estimation,” in preparation for *IEEE Trans. on Signal Processing*.

[15] L. Borcea, C. Tsogka, G. Papanicolaou, and J. Berryman, “Imaging and time reversal in random media,” *Inverse Problems*, vol. 18, pp. 1247-1279, 2002.

[16] A. J. Devaney, “Super-resolution processing of multi-static data using time reversal and MUSIC,” *J. Acoust. Soc. Am.*, to appear.

[17] P. Stoica and A. Nehorai, “MUSIC, maximum likelihood and Cramér-Rao bound,” *IEEE Trans. Acoust., Speech, Signal Processing*, vol. ASSP-37, pp. 720-741, May 1989.

[18] S. M. Kay, *Fundamentals of Statistical Signal Processing: Estimation Theory*, Englewood Cliffs, NJ: Prentice Hall, 1993.

[19] J. W. Brewer, “Kronecker products and matrix calculus in system theory,” *IEEE Transactions on Circuits and Systems*, vol. cas-25, no. 9 pp. 772-781, Sep. 1978.

[20] P. Sheng, *Introduction to Wave Scattering, Localization, and Mesoscopic Phenomena*, San Diego: Academic Press, Inc., 1995.

[21] G. Shi, A. Nehorai, “Macrocell multiple-input multiple-output system analysis,” to appear in *IEEE Trans. Wireless Communications*.